Exploring the Potential of a Plant Extract in Mitigating Corrosion under Jet Impingement Conditions

Mulky, Lavanya
Department of Chemical Engineering, Manipal Institute of Technology, Manipal Academy of Higher Education, Manipal, Karnataka, INDIA

Rao, Padmalatha*+
Department of Chemistry, Nitte Meenakshi Institute of Technology, Bangalore, Karnataka, INDIA

ABSTRACT: *The inhibition effect of Bhumyamalakhi (Phyllanthus Niruri) on 6061 aluminium alloy erosion-corrosion in simulated seawater was explored using potentiodynamic polarisation (PDP) and electrochemical impedance spectroscopy (EIS) techniques. Experiments were performed to examine the hydrodynamic effects on the behavior of the inhibitor. Conditions were optimized to achieve maximum inhibition efficiency by varying the concentration of inhibitor (500 and 1000ppm), temperature (30 ℃, 40 ℃, 50 ℃) and flowrate (4, 8, 12 L/min) of slurry. Surface morphology was studied with Scanning Electron Microscopy (SEM) and Energy Dispersion X ray (EDX) studies. The experimental findings indicated that an increase in flowrate and temperature decreased the efficiency of inhibitor and an increase in inhibitor concentration caused an increase in inhibitor efficiency. The inhibition efficiency of 80% and 53% was obtained at 30 °C and 50 ℃ at 4 L/min for 1000 ppm of inhibitor. Surface morphology demonstrated the complete damage of the material due to erosion corrosion and the surface became relatively smooth after the addition of the inhibitor.*

KEYWORDS: *Erosion corrosion; Impingement; Flowrate; Green inhibitor, Potentiodynamic polarization.*

INTRODUCTION

Erosion-corrosion is a complex phenomenon that involves the metal surface experiencing electrochemical corrosion reactions in the presence of free-flowing liquid. Solid particles present in the artificial slurry gradually and mechanically remove material from the exposed surface. Corrosion and erosion mutually reinforce one another in this process, causing the target material to sustain damage that is significantly larger overall than the combined damage caused by the individual processes [1].

Corrosion is generally obstructed by the flow due to the mass transport process. Since transport is the factor that determines corrosion rate, a turbulent flow speeds up the transfer of species to and from the metal surface [2] Turbulent flow is equally responsible for the detachment of otherwise passive film on the surface of the metal. It may also disengage the corrosion product that is deposited on the metal. All these synergistically increase the rate of erosion-corrosion.

* *To whom correspondence should be addressed.*
+ *E-mail: padmalatha.rao@nmit.ac.in*
1021-9986/2023/11/3887-3897 11/$/6.01

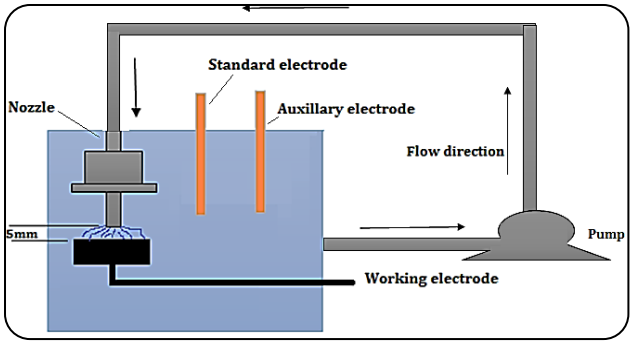

Fig. 1: Experimental rig for erosion corrosion studies

Erosion-corrosion results in the early failure of flow handling components. In industrial settings, all practical piping systems function in turbulent flow conditions, where erosion-corrosion also exists in addition to localised corrosion [3]. The rate of overall erosion-corrosion may be larger than the cumulative rates of each process operating separately because of the link between the mechanical erosion process and the electrochemical corrosion process [4]. Past studies on a number of materials have shown that rates of material loss can elevate when corrosion is aided by mechanical wear. Early equipment failures in the processing industry have been documented as a result of mechanical-electrochemical interactions [5-11].

The use of aluminium and its alloys is widespread in a number of sectors, including construction, electrical power generation, automotive, and aerospace [12]. Aluminium is resistant to corrosion because of the strong oxide film that is produced on its surface. However, this protective oxide coating can be destroyed via amalgamation or interaction with halogen, hot alkalis acids, and even water attack [13]. Numerous studies have examined electrochemical techniques under impingement jet systems, wet erosion test rigs, mass loss measurements, and erosion-corrosion damage to aluminium alloys [14-16]. In addition to the material variables, the influencing components also include fluid-related parameters such as flow velocity, impact angle, liquid phase corrosivity, flow regime and content of solid particles [17].

The problems caused by erosion-corrosion motivate researchers to develop some techniques to reduce its impact. An efficient way to manage erosion-corrosion is the addition of corrosion inhibitors [18]. Corrosion inhibitors decrease the rate of material deterioration and shield metal surfaces from corrosive attack [19]. Sand is frequently created alongside industrial fluids, and since mechanical erosion also contributes to the deterioration process, the process can be sped up by the availability of solid particles in the environment [20]. In fluids with high flow velocity and sand particles, the inhibitory activity may be decreased due to difficulties in inhibitor adsorption or damage to the generated inhibitor layer [21].

Substantial attempts have been made to comprehend the mechanical erosion behaviour of metals. The complexity of tribological systems in the industry has caused much of the research to be concentrated on particular test equipment/parameters duplicating certain field circumstances [22].

This study aims to investigate the influence of hydrodynamics on Bhumyamalakhi when applied for corrosion mitigation in 6061 aluminium alloy using an impingement jet system integrated with electrochemical measurements and surface characterisation.

EXPERIMENTAL SECTION

Experimental setup

The experimental apparatus included a reservoir tank, a temperature controller, a flowrate controller, a pump, a thermocouple, and valves. The rig was equipped with an electrochemical cell. The electrochemical cell consisted of a working electrode (6061 aluminium alloy), a reference electrode (saturated calomel electrode), and an auxiliary electrode (Pt). The potential was measured concerning the saturated calomel electrode. The auxiliary electrode helps to maintain a constant potential difference between the working electrode and the reference electrode. The slurry was pumped via a recirculating loop by a centrifugal pump, leaving the 8 mm diameter nozzle to strike the specimen in a perpendicular direction. The specimen was kept 5 mm away from the nozzle [23]. A slurry impinging jet produced by the recirculating liquid-solid impingement setup was then used to test the specimen. Artificial saltwater was created as per ASTM specifications (D1141-98) [24]. The working electrode was positioned beneath the jet at a 90° angle. The experimental setup is shown schematically in Fig 1.

Sample composition

The metal samples were extracted from a cylindrical rod with a 12-mm diameter. The samples were cleansed using acetone and dried with hot air after having their surfaces polished with emery sheets up to 600 grit level. The specimen's visible surface area was 1.11 cm^2. In each

Table 1: The nominal compositions of 6061 aluminium alloy

Elements	Mg	Si	Fe	Cu	Cr	Al
Composition (%wt)	0.96	0.80	0.40	0.27	0.21	balance

experiment, sand with an average particle size of 300 microns was added. Table 1 provides the working electrode's chemical composition.

Inhibitor

Bhumyamalakhi (*Phyllanthus niruri)* is used in several Ayurveda medicines to treat skin diseases, diabetes, and other ailments. Several biologically active compounds are present in *Phyllanthus niruri* [25]. Lignans, tannins, alkaloids, flavonoids, coumarins, saponins, terpenes, and phenylpropanoids have all been identified in the stem, leaves, and roots of *P. niruri* and have been linked to the biological activity of this plant. [26]. Numerous substances, including phyllanthin, flavonoids, tannins, glycosinoids, and hypophyllanthin, are present in the extracts and help to reduce corrosion [27]. Compounds such as phenol, flavonoid, saponin, alkaloid, and terpenoid are responsible for antioxidant and antibacterial activity [28]. Compounds containing phenolic OH group act as corrosion inhibitors by adsorption on metal surfaces when exposed to metal/solution interface [29]. Different organic compounds, alkaloids, tannins, and pigments are found in natural goods derived from plants, and the majority of them are recognized to have corrosion-inhibiting properties [30].

Potentiodynamic polarisation (PDP) studies

Potentiodynamic polarization studies were carried out using an electrochemical workstation (CH-600 D-Series US, with beta software), using a 3-electrode setup as discussed in section 2.1. OCP was determined by immersing the metal for 600 seconds. The OCP is the electrode potential measured concerning the reference electrode when there is no current flowing through it. The electrode was polarised at ±500 mv and at a scan rate of 1 mV/s to produce potentiodynamic polarisation curves.

Once each experiment is complete, the measured cathodic and anodic Tafel constants were utilized to derive the corrosion current density, (i_{corr},) using Eq. (1) [32].

$$i_{corr} = \frac{\beta}{R_{ct}} = \frac{1}{R_{ct}} \frac{\beta_a \beta_c}{2.303\ (\beta_a - \beta_c)} \quad (1)$$

Where β is the coefficient of Stern-Geary, βa, and βc are the anodic and cathodic Tafel constants. Eq. (2) is then used to get the overall corrosion rate.

$$CR\ (mm\ a^{-1}) = \frac{3270 M\, i_{corr}}{\rho Z} \quad (2)$$

Where 3270 is a constant with the unit of corrosion rate, M is the atomic mass of aluminium (M=27), ρ is the corroding material density of aluminium of 2.7 g/cm, Z is the electrons transferred per metal atom (n=3) [33].

Inhibition efficiency was calculated from the Eq. (3) [34].

$$IE\ (\%) = \frac{i_{corr.bl} - i_{corr.inh}}{i_{corr.bl}} \quad (3)$$

Where $i_{coor.bl}$ and $i_{corr\ inh}$ denotes corrosion current density in the absence and in the presence of inhibitor

Electrochemical Impedance Studies (EIS)

This is a potent technique for analyzing the precise corrosion inhibition behaviors of organic inhibitors and their protective mechanisms [35]. EIS was carried out with AC signals at the open circuit potential and in the frequency range 100 kHz to 0.01 Hz. ZSimpWin 3.2 software was used to analyze the data.

Both experiments were carried out by varying the concentration of inhibitor (500 ppm and 1000 ppm) at three different temperatures (30, 40 and 50 ℃) at the flowrate of 4, 8, and 12 L/min

Surface morphology studies

Surface morphology studies using analytical scanning electron microscopy (JEOL JSM-6380L) were carried out both with and without the inhibitor. Elemental mapping was done by EDX analysis.

RESULTS AND DISCUSSION

Effect of flowrate

The experimental results obtained from the potentiodynamic polarization studies on 6061 aluminium alloy in artificial seawater slurry are shown in Fig. 2.

Fig. 2 shows the cathodic and anodic polarisation curves recorded for erosion-corrosion of 6061 aluminium alloy after immersion in artificial seawater slurry at 30 ºC. Various electrochemical parameters obtained from PDP studies are depicted in Table 2.

In the above plot, anodic curves represent metal dissolution and a cathodic curve represents a reduction of oxygen in a neutral medium. The shape of the curve remains almost unaltered after the addition of the inhibitor. There is not much variation in the values of anodic and cathodic slopes for uninhibited and inhibited solutions. This suggested that the added inhibitor slowed down the rate of corrosion

Table 2: Electrochemical parameters from PDP measurements for corrosion of 6061 aluminium alloy in the presence and absence of 500 ppm of Bhumyamalakhi at different temperatures

Temp (K)	Flowrate (L/min)	E_{corr} (mV) (Blank)	E_{corr} (mV) (500ppm)	βa (V/dec)	-βc (V/dec)
303	4	-640	-727	0.47	0.38
	8	-672	-432	0.50	0.47
	12	-363	-439	0.52	0.45
313	4	-713	-381	0.48	0.57
	8	-639	-347	0.63	0.49
	12	-691	-651	0.52	0.21
323	4	-703	-285	0.59	0.44
	8	-602	-614	0.41	0.40
	12	-715	-513	0.48	0.45

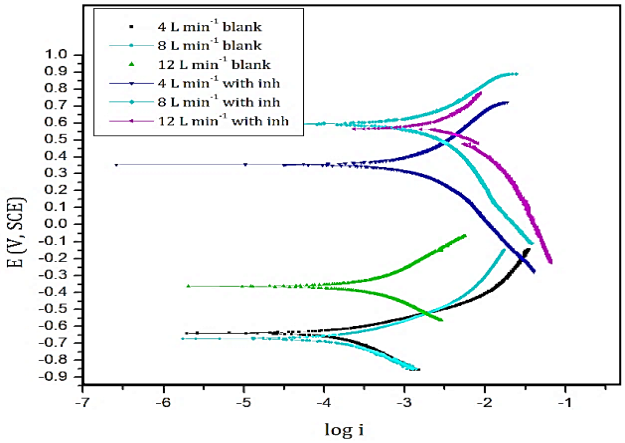

Fig. 2: PDP plots for variation in flowrate in the absence and presence of 500ppm inhibitor at 30 ℃.

without altering the mechanism. It brought down the corrosion by merely blocking the available adsorption sites. Values of inhibition efficiency under different experimental conditions are tabulated in Table 3.

Inhibition efficiency decreased with an increase in the flowrate of the slurry. This is much anticipated under turbulent conditions. Because of the greater rate of flowrate, the passive layer may break down and create more active sites. Added inhibitor may not be sufficient to bring down the expected inhibition efficiency. Further, due to the high flowrate the inhibitor film may also get detached thereby decreasing the inhibition efficiency. Temperature may also contribute similarly. [36]

Effect of sand in Artificial seawater slurry

The interaction between the sand, the inhibitor film, and the target metal is illustrated in Fig. 3. Each particle leaves

Table 3: Inhibition efficiency from PDP measurements for corrosion of 6061 aluminium alloy in the presence and absence of 500 ppm of Bhumyamalakhi at different temperatures

Temp (K)	Flowrate (L/min)	i_{corr} (mA/cm^2) (Blank)	i_{corr} (mA/cm^2) (500 ppm)	IE%
303	4	1.45	0.27	81.37
	8	2.03	0.44	78.32
	12	2.65	0.71	73.20
313	4	1.85	0.57	69.18
	8	2.50	2.41	36.00
	12	3.78	2.64	30.15
323	4	3.38	1.58	53.25
	8	3.61	2.45	32.13
	12	4.14	3.18	23.18

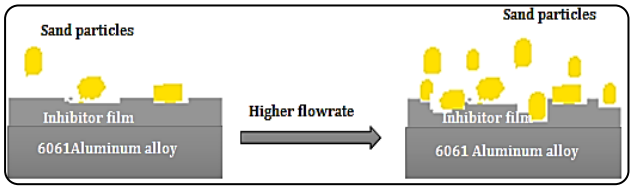

Fig. 3: Impact on the film formed over the alloy at higher flowrates

a mark on the surface, harming both the passive film as well as material surface. Corrosion might get accelerated by the disappearance of the passive coating since there is no longer a barrier to stop mass transfer over the surface. The formation of numerous micro-galvanic sites as a result of numerous particles striking the material will also enhance surface roughness (as shown in the SEM picture in Fig. 9). All of these effects accelerate corrosion process [37].

The removal of the adsorption coating brought on by fluid flow and solid particle impact lowered the corrosion inhibitors' effectiveness under erosion-corrosion circumstances [38].

The energy of the deteriorated particles and the attack's intensity, which increases with energy, determine how corrosive wear occurs. The energy of eroding particles is strongly related to the energy of impacting particles [39]. The flowrate of the inhibitor-containing solution on the metal may have two different impacts. (i) With an increase in flowrate, the fluid increases the concentration of inhibitor molecules near the substrate, which helps to increase efficiency. (ii) In a similar vein, higher flowrates may also hasten the mass transfer of corrosive species to the metal and/or increase the kinetic energy of the slurry's particles, both of which could fail the inhibitor film layer [40].

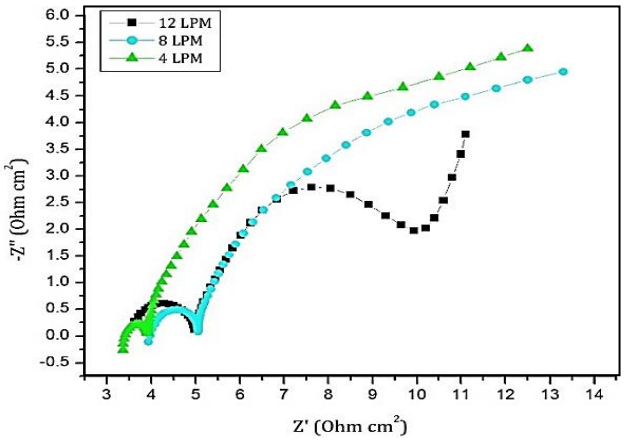

Fig. 4: Nyquist plot obtained at various flowrates after the addition of 500 ppm inhibitor at 30° C

The corrosion rate increased with the flow velocity when the inhibitor film completely covered the metal surface. This is caused by a partial erosion of the inhibitor layer [41]. The development of corrosion products may also be impacted by the inhibitor, which would further affect the corrosion processes [42]. The inhibitor physically prevents the sand impactor from working by adhering to the metal surface. As a result, erosion damage would be reduced. The solid particles also absorb the inhibitor, which lowers the speed and impact energy of the sand when it strikes the metal surface [43].

Electrochemical Impedance Studies

Electrochemical impedance analysis was carried out on 6061 aluminium alloy. Fig. 4 shows the result of electrochemical impedance studies at 30° C under various flowrate s after adding 500 ppm of the inhibitor.

The Nyquist plot illustrates the presence of three semicircles at all flowrates. All are characterized by a high-frequency capacitive loop followed by, an intermediate-frequency inductive loop which in turn is followed by a secondary capacitive loop and a tail at the end. The shape of the Nyquist plot obtained agrees very well with those reported for 6061 aluminium alloy under similar experimental conditions.

As far as frequency segmentation goes, there are three zones. The behaviour of the solution According to reported literature [44] high frequency capacitive loop stands for charge transfer resistance. As very much evident from Fig. 4, with an increase in the flowrate of slurry containing 500 ppm of inhibitor, the diameter of the semicircle decreased. Decrease in the diameter of the Nyquist plot is accompanied

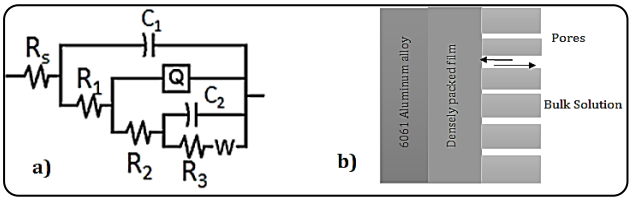

Fig. 5 (a) Simulated circuit (b) Corrosion process as explained by the simulated model

by the decrease in the inhibition efficiency. In the intermediate frequency region, there is a small inductive loop, which could be attributed to the formation of the stable protective layer. However, with increased turbulence the productive layer will be broken and the corrosion rate increases, this is indicated by the presence of a secondary capacitive loop at low frequency.

A significant diffusive tail is observed at 12 L/min flowrate. A distinctive diffusive tail was not observed at 4 and 8 L/min. At all the studied flowrates a high frequency offered a lower resistance than a low-frequency capacitive loop. However, a fall in corrosion resistance was detected at elevated flowrate s.

The simulated equivalent circuit is shown in Fig. 5. It is generally known that a homogeneous, faultless coating on a metal typically has a high impedance value, which can be depicted by a straightforward Randle's cell with a single semicircle on the Nyquist plot or by a single time constant. In a perfect scenario with a uniform coating, the oxide layer's capacitance will meld with the coatings, making it difficult to tell them apart as separate capacitive parts. There will be more than one time constant and distinct semicircle as opposed to just one, though, if the coating on the substrate develops defects and becomes porous [45].

The results from EIS studies were simulated using ZSimpWin 3.2 software, and the following circuits were obtained. The equivalent circuit in Fig. 5 (a) – *(C1-R1)* represents the non-stable porous corrosion product layer. *(Q-R2)* represents the densely packed corrosion product layer. Instead of using double-layer capacitance, Constant Phase Element (CPE) was employed to fit the experimental results better [46]. In *(C2-R3) C2* is the double-layer capacitance, and *R3* is the charge transfer resistance. Warburg impedance in the circuit relates to the diffusion of the ions through the pores. Some insoluble corrosion products may be separated from the aluminium surface due to shear stresses through hydrodynamic conditions, further increasing the corrosion rate. An inductive loop that appears in the low-frequency band demonstrates these occurrences.

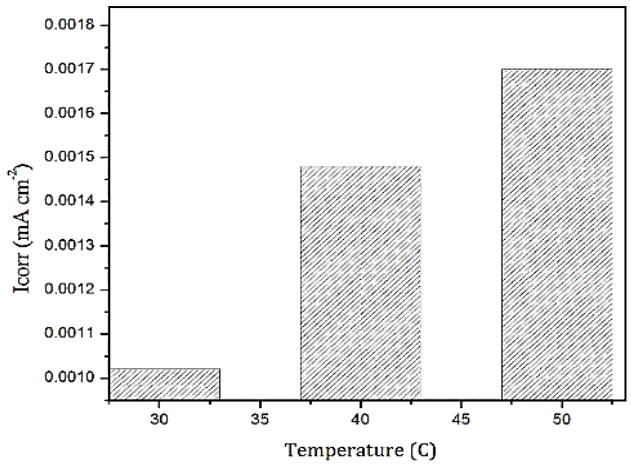

Fig. 6: Increase in corrosion rate after the addition of 500 ppm inhibitor with the increase in temperature

To analyse data for rough solid electrodes, the CPE is frequently utilised [47]. The impedance, *Z*, of the CPE is determined by Eq. (4).

$$Z_{CPE} = \frac{1}{y_0 j^n_w} \quad (4)$$

Where, y_o signifies the CPE constant, ω is the angular frequency, j represents the imaginary number (i.e. $i^2 = -1$), and n is the exponent (phase shift) which measures surface in-homogeneity [48].

The corrosion product layer and inhibitor film are substantially impacted by the flow velocity and the presence of sand particles. These particles can produce considerable local pressures when they come into contact with a metal surface, and the high-velocity sand can dissolve the corrosion product layer. Additionally, the flow and sand particles that come into contact with the metal surface may remove some inhibitor molecules from it [32].

Effect of temperature

Understanding the inhibitive mechanism of the process of corrosion depends critically on temperature. Experiments were conducted at 30 – 50 °C in inhibited solutions with 500 ppm and 1000 ppm concentrations of Bhumyamalakhi, and the corrosion rate was assessed to determine the impact of temperature.

Even at 1000 ppm inhibitor concentration of Bhumyamalakhi similar results were observed. With the increase in temperature, the rate of corrosion accelerated. This indicated that, as the temperature rises, the inhibitor efficiency decreases, as illustrated in Fig. 6. When the temperature rises, owing to a reduction in surface coverage,

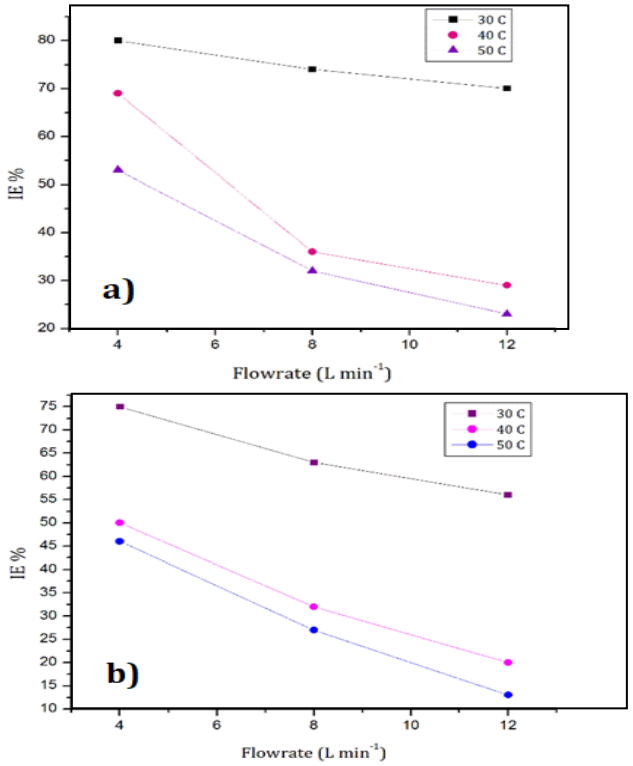

Fig. 7: Variation of inhibition efficiency with flowrate (a) 500 ppm (b) 1000 ppm of inhibitor

the surface of the aluminium alloy is exposed to the corrosive environment. It causes the inhibitor molecule to desorb from the surface. This can be because the adsorption mechanism loses strength at higher temperatures [49].

It can be observed from Fig. 7 that there is a decrease in the anti-corrosion efficiency with the increase in the flowrate. Though the % IE (Inhibition Efficiency) was greater at a higher inhibitor concentration, the trend almost remained the same. This can be caused by the excessive addition of inhibitors to the medium, and the corrosion rate will be negatively impacted by that particular concentration of Bhumyamalakhi.

The corrosion inhibition efficiency did not significantly increase at temperatures beyond 50°C, however, because the corrosion rate likewise increased as the temperature rose. Temperature-dependent variations in the percentage of inhibition in the presence of this inhibitor imply that physical adsorption was the primary mechanism of inhibition because the amount of adsorbed inhibitor reduces as temperature rises [50]. This result also showed that the adhesion of inhibitor molecules to the aluminium alloy's surface was an exothermic process.

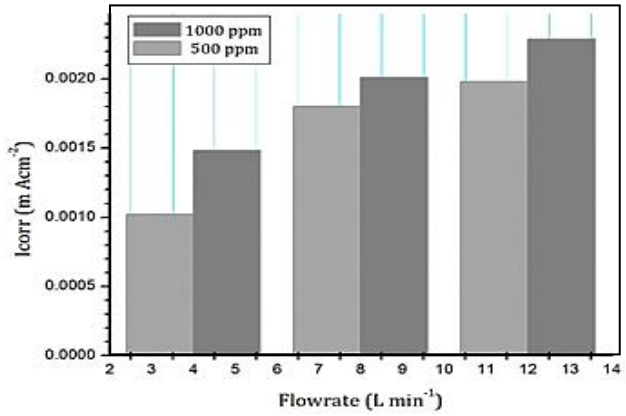

Fig. 8: Corrosion rate of 6061 aluminium alloy at various flowrates and concentrations

Effect of inhibitor concentration

The corrosion rate decreased when the inhibitor concentration was raised from 500 ppm to 1000 ppm, as depicted in Fig. 8. But the trend of corrosion rate variation conceming the flowrate remained the same. The corrosion rate of 6061 aluminium alloy depends on the concentration of inhibitors. For Bhumyamalakhi, when the concentration changed, the inhibition performance changed significantly.

According to the findings in Fig. 8, corrosion current density (i_{corr}) falls with increase in concentration of the inhibitor. This type of behaviour could be explained by a strong interaction between inhibitor molecules and the alloy surface. This suggested that inhibitor molecules have adhered to the alloy surface and are creating a barrier on the surface of the mild steel [51]. Adsorbate inhibitor molecules align parallel to the metal surface at inhibitor concentrations lower than 1000 ppm, which reduces the number of active surface sites [52]. The amount of inhibitor molecules that can adsorb on the metal surface increases with increasing inhibitor concentration, up to a concentration of 1000 ppm. On the other hand, as inhibitor concentration increased, inhibitor molecules were more strongly attracted to one another. Additionally, the molecules tended to adsorb onto the metal surface as inhibitor concentration reached a critical point because of the electrostatic repelling effect perpendicularly. Each adsorbate inhibitor molecule with perpendicular adsorption at a greater concentration would occupy a smaller surface area than with parallel adsorption, leading to a considerable increase in corrosion rate [27].

Inhibitor molecules repel one another more powerfully when inhibitor concentration rises. The electrostatic repellent property of the molecules then caused them to tend to adsorb perpendicularly onto the metal surface. In contrast to a paralleled alignment, each inhibitor molecule would occupy a reduced surface area in this scenario. The inhibitor's ability to work with corrosion products created on the surface of the metal is a likely explanation. More so than the inhibitor layer itself, the corrosion product molecules can persist on the metal surface, which lessens the influence of sand on the surface.

Scanning electron microscopy

SEM investigated the morphology of the alloy surface before and after impingement. Fig 9 (a) and (b). Material has undergone substantial degradation after impingement as visible in Fig 9(b) The craters and protruding lips on the surface are most likely the result of multiple overlapping collisions. In comparison to the samples given to lower velocities, the specimen subjected to the highest velocity exhibits greater plastic deformation. It also exhibits the greatest density and depth of impact craters and surface lips. A portion of the kinetic energy of the particles that are taken up by the sample surface during the impingement process result in plastic deformation, which eventually creates a coating that hardens with use.

It is discovered that more deformation caused by the sand particles' enhanced flowrate and kinetic energy results in deeper cuts and fissures on the surface as well as greater material loss. The particle damaged the material surface by slamming against it perpendicularly at 90 degrees, creating a small pothole. Due to the variation in particle size, when the following particle is hit on the pit, it may appear in two places. As seen in Fig. 9, when the particle diameter was greater than the pit, the erosion-corrosion process produced microcracks as a result of the sharp edges of the abrasive particles. Chloride ions entering the sample caused corrosion products to develop inside the microcracks, causing tensile strains that enlarged the fissures. Particles fell vertically into the pit when their diameter was less than that of the pit. Particles would degrade the substance and create an environment where chloride ions would produce pitting when they collide with the hole [53]. After the addition of inhibitor material has become relatively smooth due to the deposition of the inhibitor.

EDX Analysis

Elemental mapping was performed to demonstrate the presence and distribution of different elements on the alloy's surface. In Fig. 10, a significant amount of oxygen and carbon

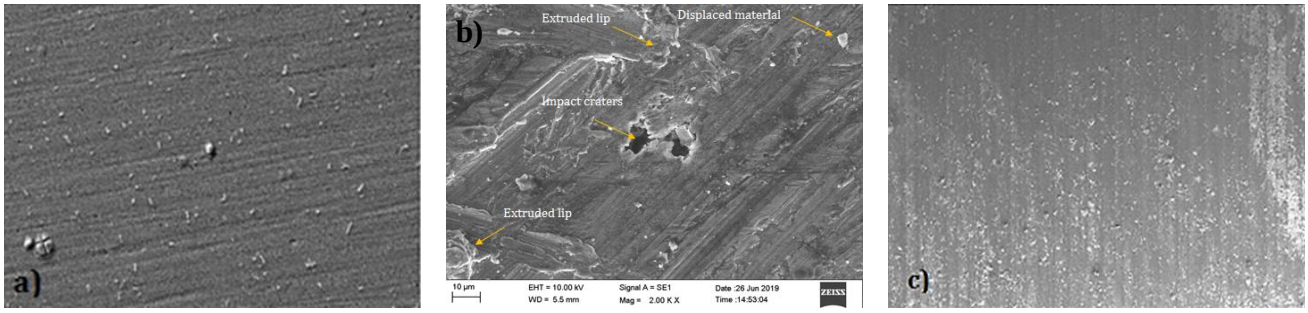

Fig. 9: Scanning electron microscopy micrographs at 12 L/min and 50 °C illustrating craters and lips generated on the 6061 aluminium alloy surface

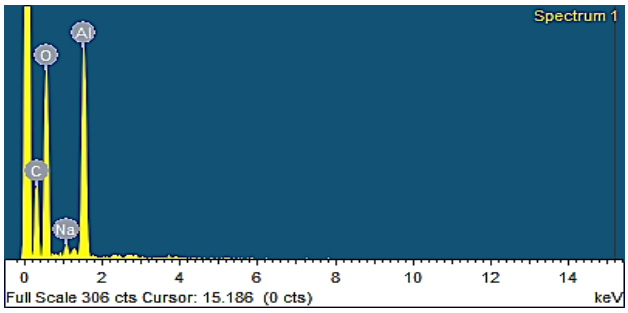

Fig. 10: EDX maps recorded for aluminium alloy after the addition of the inhibitor at 40° C and 12 L/min

was observed. The presence of oxygen and carbon indicates the adsorption of inhibitor molecules which contain a large number of electron-rich oxygen atoms. The presence of carbon is mainly due to the backbone of the inhibitor molecule.

CONCLUSIONS

- This study made use of Bhumyamalakhi plant extract to study its inhibition towards corrosion on 6061 aluminium alloy in simulated seawater.
- The reduction in corrosion rate and current density (i_{corr}) with all tested inhibitor concentrations demonstrated that Bhumyamalakhi operates as an efficient inhibitor for aluminium alloy in an artificial seawater environment.
- The erosion-corrosion process was activation-controlled and diffusion-controlled as indicated by electrochemical impedance studies.
- It was observed that the inhibitor concentration, temperature, and flowrate all affected inhibition efficiency.
- Surface studies and elemental mapping confirmed the adsorption of inhibitor onto the surface of the metal.

Future Scope

Individual components of the extract can be investigated for its potency against erosion-corrosion inhibition. Further its effect on corrosion and erosion may be individually evaluated to check for synergy. Plant extract nanoparticles can be evaluated for erosion corrosion protection. Plant extract in the form of coatings can be explored.

Nomenclature

Potentiodynamic Polarization	PDP
The Submerged Jet Impingement	SJI
Corrosion Resistance	CR
Inhibition Efficiency	IE
Saturated Calomel Electrode	SCE
Open Circuit Potential	OCP
Electrochemical Impedance Spectroscopy	EIS
Constant Phase Element	CPE
Scanning Electron Microscope	SEM
Energy Dispersive X-Ray	EDX
Corrosion Current Density	i_{corr}

Received: Dec. 31, 2022; Accepted: May. 29, 2023

REFERENCES

[1] Javaheri V., Porter D., Kuokkala V.T., Slurry Erosion of Steel – Review of Tests, Mechanisms and Materials, *Wear*, **408–409:** 248–273 (2018).

[2] Silva C.A., Varela L.B., Kolawole F.O., Tschiptschin A.P., Panossian Z., Multiphase-Flow-Induced Corrosion and Cavitation-Erosion Damages of API 5L X80 and API 5DP Grade S Steels, *Wear*, **452–453:** 203282 (2020).

[3] Lavanya M., Murthy V.R., Rao P., Erosion Corrosion Control of 6061 Aluminium Alloy in Multi-Phase Jet Impingement Conditions with Eco-Friendly Green Inhibitor, *Chin. J. Chem. Eng.*, **28(2):** 340–347 (2020).

[4] Liu Y., Alfantazi A., Schaller R.F., Asselin E., Localised Instability of Titanium during its Erosion-Corrosion in Simulated Acidic Hydrometallurgical Slurries, *Corros. Sci.*, **174:** 108816 (2020).

[5] Aguirre J., Walczak M., Effect of Dissolved Copper Ions on Erosion–Corrosion Synergy of X65 Steel in Simulated Copper Tailing Slurry, *Tribol. Int.*, **114:** 329–336 (2017).

[6] Barik R.C., Wharton J.A., Wood R.J.K., Stokes K.R., Electro-Mechanical Interactions during Erosion–Corrosion, *Wear*, **267(11):** 1900–1908 (2009).

[7] Soliz Á., Cáceres L., Pineda F., Galleguillos F., Erosion–Corrosion of AISI 304L Stainless Steel Affected by Industrial Copper Tailings, *Metals*, **10(5):** 1005 (2020).

[8] Zhao Y.L., Ye F.X., Zhang G., Yao J., Liu Y.F., Dong S.G., Investigation of Erosion-Corrosion Behavior of Q235B Steel in Liquid-Solid Flows, *Pet. Sci.*, **19(5):** 2358–2373 (2022).

[9] Ramírez-Arreola D.E., Aranda-García F.J., Sedano-de la Rosa C., Vite-Torres M., Gallardo-Hernández E.A., Godínez-Salcedo J.G., Influence of Swirl Number and Incidence Angle on Erosion-Corrosion Behavior of API 5L X-52 Steel under Swirling Jets, *Wear*, **510–511:** 204518 (2022).

[10] Zhou H., Ji Q., Liu W., Ma H., Lei Y., Zhu K., Experimental Study on Erosion-Corrosion Behavior of Liquid-Solid Swirling Flow in Pipeline, *Mater. Des.*, **214:** 110376 (2022).

[11] Du Y., Yang G., Chen S., Ren Y., Research on the Erosion-Corrosion Mechanism of 304 Stainless Steel Pipeline of Mine Water in Falling Film Flow, *Corros. Sci.*, **206:** 110531 (2022).

[12] Chaubey N., Savita, Singh V.K., Quraishi M.A., Corrosion Inhibition Performance of Different Bark Extracts on Aluminium in Alkaline Solution, *J. Asso. Arab Univer. Basic App. Sci.*, **22:** 38–44 (2017).

[13] Afzal S.N., Shaikh M.A.A., Mustafa C.M., Nabi M., Ehsan M.Q., Khan A.H., Study of Aluminium Corrosion in Chloride and Nitrate Media and Its Inhibition by Nitrite, *J. Nepal Chem. Soc.*, **22:** 26–33 (2007).

[14] Yadav P.K., Dixit G., Investigation of Erosion-Corrosion of Aluminium Alloy Composites: Influence of Slurry Composition and Speed in a Different Mediums, *J. King Saud. Univ. Sci.*, **31(4):** 674–683 (2019).

[15] Saxena M., Modi O.P., Prasad B.K., Jha A.K., Erosion and Corrosion Characteristics of an Aluminium Alloy-Alumina Fibre Composite, *Wear*, **169(1):** 119–124 (1993).

[16] Ramesh N.R., Kumar V.S.S., Experimental Erosion-Corrosion Analysis of Friction Stir Welding of AA 5083 and AA 6061 for Sub-Sea Applications, *Applied Ocean Research*, **98:** 102121 (2020).

[17] Wang Z.B., Zheng Y.G., Critical Flow Velocity Phenomenon in Erosion-Corrosion of Pipelines: Determination Methods, Mechanisms and Applications, *J. Pipe. Sci. Eng.*, **1(1):** 63–73 (2021).

[18] Deyab M.A., The Effect of Disodium Cocoamphodiacetate on Corrosion-Erosion Resistance of Steel in Saline Water, *J. Mol. Liq.*, **271:** 240–245 (2018).

[19] Ituen E., Mkpenie V., Yuanhua L., Singh A., Inhibition of Erosion Corrosion of Pipework Steel in Descaling Solution Using 5-Hydroxytryptamine-based Additives: Empirical and Computational Studies, *J. Mol. Struct.*, **1204: 127562:** (2020).

[20] Senatore E.V., Pinto M.C.P., Souza E.A., Barker R., Neville A., Gomes J.A.C.P., Effects of Pre-Filmed $FeCO_3$ on Flow-Induced Corrosion and Erosion-Corrosion in the Absence and Presence of Corrosion Inhibitor at 60 °C, *Wear*, **480–481:** 203927 (2021).

[21] Zeng L., Guo X.P., Zhang G.A., Inhibition of the Erosion-Corrosion of a 90° Low Alloy Steel Bend, *J. Alloys. Compd.*, **724:** 827–840: (2017).

[22] Chung R.J., Jiang J., Pang C., Yu B., Eadie R., Li D.Y., Erosion-Corrosion Behaviour of Steels Used in Slurry Pipelines, *Wear*, **477:** 203771 (2021).

[23] Lavanya M., Murthy V.R., Rao P., Electrochemical Investigation of Erosion-Corrosion Behavior of 6061 Aluminium Alloy in Marine Environment, *Tribology in Industry*, **40(4):** 552–564 (2018).

[24] "Designation: D 1141-98 (Reapproved 2003) Standard Practice for the Preparation of Substitute Ocean Water 1" An American National Standard, ASTM (2003)

[25] Zhu X., Pathakoti K., Hwang H.M., "Green Synthesis of Titanium Dioxide and Zinc Oxide Nanoparticles and their Usage for Antimicrobial Applications and Environmental Remediation" Green Synthesis, Characterization and Applications of Nanoparticles, Elsevier, 223–263 (2019).

[26] Bagalkotkar G., Sagineedu S.R., Saad M.S., Stanslas J., Phytochemicals from Phyllanthus niruri Linn. and their Pharmacological Properties: A Review, *J. Phar. Phar.*, **58(12):** 1559–1570 (2010).

[27] Haseena S., *et al.*, Investigation on Photocatalytic Activity of Bio-Treated α-Fe_2O_3 Nanoparticles Using Phyllanthus niruri and Moringa Stenopetala Leaf Extract Against Methylene Blue and Phenol Molecules: Kinetics, Mechanism and Stability, *J. Environ. Chem. Eng.*, **9(1):** 104996 (2021).

[28] Ramandeep K., Akhtar N., Neelabh C., Kumar N., Phytochemical Screening of Phyllanthus niruri collected from Kerala Region and its Antioxidant and Antimicrobial Potentials, *Journal of Pharmaceutical Sciences and Research*, **9(8):** 1312–1316 (2017).

[29] Rodge J.K., Muley M.R., Kulkarni D.R., Deshpande M.N., Inhibition Effects of Phenols on Corrosion of Mild Steel in Nitric Acid, *Asian Journal of Chemistry*, **19(6):** 4745–4752 (2007).

[30] Chihi S., Gherraf N., Alabed B., Hameurlain S., Inhibition Effect of Flavonoid Extract of Euphorbia Guyoniana on the Corrosion of Mild Steel in H_2SO_4 Medium, *J. Funda. Appl. Sci.*, **1(2):** 31–39 (2009).

[31] Mulky L., Murthy V.R., Rao P., An Insight into Inhibitory Performance of Commiphora Mukul on Corrosion of Aluminium Alloy under Tribological Conditions, *Journal of the Iranian Chemical Society*, **18(11):** 2953–2963 (2021).

[32] Senatore E.V., et al., Evaluation of High Shear Inhibitor Performance in CO_2-Containing Flow-Induced Corrosion and Erosion-Corrosion Environments in the Presence and Absence of Iron Carbonate Films, *Wear*, **404–405:** 143–152 (2018).

[33] B.P. C., Rao P., An Ecofriendly Approach for Corrosion Control of 6061 Al-15%(v) SiC(P) Composite and its Base Alloy, *Chin. J. Chem. Eng.*, **25(3):** 372 (2017).

[34] Chen L., Su R.K.L., Corrosion Rate Measurement by Using Polarization Resistance Method for Microcell and Macrocell Corrosion: Theoretical Analysis and Experimental Work with Simulated Concrete Pore Solution, *Constr. Build. Mater.*, **267:** 121003 (2021).

[35] Ricky E.X., Mpelwa M., Xu X., The Study of m-Pentadecylphenol on the Inhibition of Mild Steel Corrosion in 1 M HCl Solution, *Journal of Industrial and Engineering Chemistry*, **101:** 359–371 (2021).

[36] Stack M.M., Abd El-Badia T.M., Some Comments on Mapping the Combined Effects of Slurry Concentration, Impact Velocity and Electrochemical Potential on the Erosion–Corrosion of WC/Co–Cr Coatings, *Wear*, **264(9-10):** 826–837 (2008).

[37] Rajahram S.S., Harvey T.J., Wood R.J.K., Electrochemical Investigation of Erosion–Corrosion Using a Slurry Pot Erosion Tester, *Tribol. Int.*, **44(3):** 232–240 (2011).

[38] Wang Z.B., Zheng Y.G., Critical Flow Velocity Phenomenon in Erosion-Corrosion of Pipelines: Determination Methods, Mechanisms and Applications, *J. Pipe. Sci. Eng.*, **1(1):** 63–73 (2021).

[39] Yadav P.K., Dixit G., Investigation of Erosion-Corrosion of Aluminium Alloy Composites: Influence of Slurry Composition and Speed in a Different Mediums, *J. King Saud. Univ. Sci.*, **31(4):** 674–683 (2019).

[40] Lavanya M., Murthy V.R., Rao P., Performance Evaluation of a Potent Green Inhibitor on 6061 Aluminium Alloy Under Liquid/Solid Jet Impingement, *J. Bio. Tribocorros.*, **5(4):** 1–10 (2019).

[41] Barmatov E., Hughes T., Nagl M., Efficiency of Film-Forming Corrosion Inhibitors in Strong Hydrochloric Acid under Laminar and Turbulent Flow Conditions, *Corros. Sci.*, **92:** 85–94 (2015).

[42] Neville A., Wang C., Erosion–Corrosion of Engineering Steels—Can it be Managed by Use of Chemicals?, *Wear*, **267(11):** 2018–2026 (2009).

[43] Teymouri F., Allahkaram S.R., Shekarchi M., Azamian I., Johari M., A Comprehensive Study on the Inhibition Behaviour of Four Carboxylate-based Corrosion Inhibitors Focusing on Efficiency Drop after the Optimum Concentration for Carbon Steel in the Simulated Concrete Pore Solution, *Constr. Build. Mater.*, **296:** 123702 (2021).

[44] Jakeria M.R., Ward L., Cole I., Long Term Durability Studies on the Corrosion Inhibition Effect of 2-Mercaptobenzimidazole ($C_3H_4N_2S$) on AA6022: Mechanism of Film Formation and Influence of IMPs, *Surfaces and Interfaces*, **25:** 101164 (2021).

[45] Verma C., Quraishi M.A., Kluza K., Makowska-Janusik M., Olasunkanmi L.O., Ebenso E.E., Corrosion Inhibition of Mild Steel in 1M HCl by D-Glucose Derivatives of Dihydropyrido [2,3-d:6,5-d′] Dipyrimidine-2, 4, 6, 8(1H,3H, 5H,7H)-Tetraone, *Scientific Reports*, **7(1):** 1–17 (2017).

[46] Jiang B., Sun W., Cai J., Chen S., Hou B., Inhibition of Carbon Steel Corrosion in HCl Solution Using N-Oleyl-1,3-Propanediamine based Formulation, *Colloids Surf. A Physicochem Eng. Asp.*, **624:** 126824 (2021).

[47] Ashassi-Sorkhabi H., Kazempour A., Chitosan, its Derivatives and Composites with Superior Potentials for the Corrosion Protection of Steel Alloys: A Comprehensive Review, *Carbohydr. Polym.*, **237:** 116110 (2020).

[48] Shukla S.K., Ebenso E.E., Corrosion Inhibition, Adsorption Behavior and Thermodynamic Properties of Streptomycin on Mild Steel in Hydrochloric Acid Medium, *Int. J. Electrochem. Sci*, **6:** 3277–3291 (2011).

[49] Nahlé A., Abu-Abdoun I.I., Abdel-Rahman I., Effect of Temperature on the Corrosion Inhibition of Trans-4-Hydroxy-4 ′-Stilbazole on Mild Steel in HCl Solution, *International Journal of Corrosion*, **2012:** 380329 (2012).

[50] Farhadian A., Rahimi A., Safaei N., Shaabani A., Abdouss M., Alavi A., A Theoretical and Experimental Study of Castor Oil-based Inhibitor for Corrosion Inhibition of Mild Steel in Acidic Medium at Elevated Temperatures, *Corros. Sci.*, **175:** 108871 (2020).

[51] Jiang X., Zheng Y.G., Ke W., Effect of Flow Velocity and Entrained Sand on Inhibition Performances of Two Inhibitors for CO_2 Corrosion of N80 Steel in 3% NaCl Solution, *Corros. Sci.*, **47(11):** 2636–2658 (2005).

[52] Ramachandran S., Campbell S., Ward M.B., "The Interactions and Properties of Corrosion Inhibitors with Byproduct Layers", *CORROSION*, NAC-00025, Orlando, Florida, USA, (2000).

[53] Liu Y., Zhao Y., Yao J., Synergistic Erosion–Corrosion Behavior of X80 Pipeline Steel at Various Impingement Angles in Two-Phase Flow Impingement, *Wear*, **466–467:** 203572 (2021).